Earth Surface Processes and Landforms
Earth Surf. Process. Landforms **26**, 553–576 (2001)

MODELLING THREE-DIMENSIONAL FLOW STRUCTURES AND PATTERNS OF BOUNDARY SHEAR STRESS IN A NATURAL POOL–RIFFLE SEQUENCE

D. J. BOOKER, D. A. SEAR* AND A. J. PAYNE
Department of Geography, University of Southampton, Highfield, Southampton, SO17 1BJ, UK

Received 1 February 2000; Revised 14 August 2000; Accepted 18 September 2000

ABSTRACT

Fluid–sediment interactions control river channel forms and processes. Analysis of spatial hydraulic patterns and the resulting boundary shear stress are required to aid understanding of river system behaviour. In this paper, the hydraulic processes active in a natural pool–riffle sequence are simulated using a three-dimensional computational fluid dynamics (CFD) model. Methods employed for the prescription of model boundary conditions are outlined. Model calculations are assessed using comparisons with field observations acquired over a range of flows. Simulations are then used to illustrate flow structures and patterns of boundary shear stress for a near-bankfull and an intermediate flow event. Results are used to assess existing theories that seek to explain the development and maintenance of pool–riffle sequences. Simulated results suggest that near-bed velocities and bed shear stresses decrease on riffles and increase in pools as discharge increases. Model simulations indicate that secondary flow acts to route near-bed flow over the downstream side of riffles and into the pool-head away from the centre of pools. Implications for sediment transport and pool maintenance are discussed. Copyright © 2001 John Wiley & Sons, Ltd.

KEY WORDS: pool–riffle; CFD; hydraulics; modelling

INTRODUCTION

Three-dimensional computational fluid dynamic (CFD) modelling can be used to simulate hydraulic patterns in natural river channels allowing improved simulation of key processes (Lane, 1998). Numerical models, tested using field data, may be capable of replicating velocity patterns and secondary structures in complex natural channels (Olsen and Stokseth, 1995; Lane and Richards, 1998; Hodskinson and Ferguson, 1998; Nicholas and Sambrook-Smith, 1999). This paper describes the use of a CFD model and the resulting patterns of flow and boundary shear stress in a channel containing four pool–riffle sequences. Pool–riffle sequences are a fundamental component of the fluid–sediment interactions that control bed scour, sediment transfer and deposition in rivers (Keller, 1971; Richards, 1976; Carling, 1991). Moves towards 'environmentally sensitive engineering' (Hey, 1992; Brookes, 1995) and river restoration (Brookes, 1996; Sear *et al.*, 1995) have highlighted the need for increased understanding of flow structures and sediment dynamics in pool–riffle sequences. The aim of this paper is to analyse hydraulic patterns in a natural pool–riffle sequence with a view to explaining the maintenance of pool–riffle morphology. Recent investigations have stressed the importance of combinations of hydraulic and sedimentological process interaction (e.g. Clifford, 1993; Sear, 1996). Whilst recognizing that theories based on spatial patterns in sedimentological structure exist, this paper will concentrate on hydraulic rather than sedimentological explanations.

CURRENT THEORIES EXPLAINING POOLS AND RIFFLES

Despite a lack of spatially distributed hydraulic field observations, hydraulic-based theories have been

* Correspondence to: D. A. Sear, Department of Geography, University of Southampton, Highfield, Southampton, SO17 1BJ, UK.
E-mail: D.Sear@soton.ac.uk

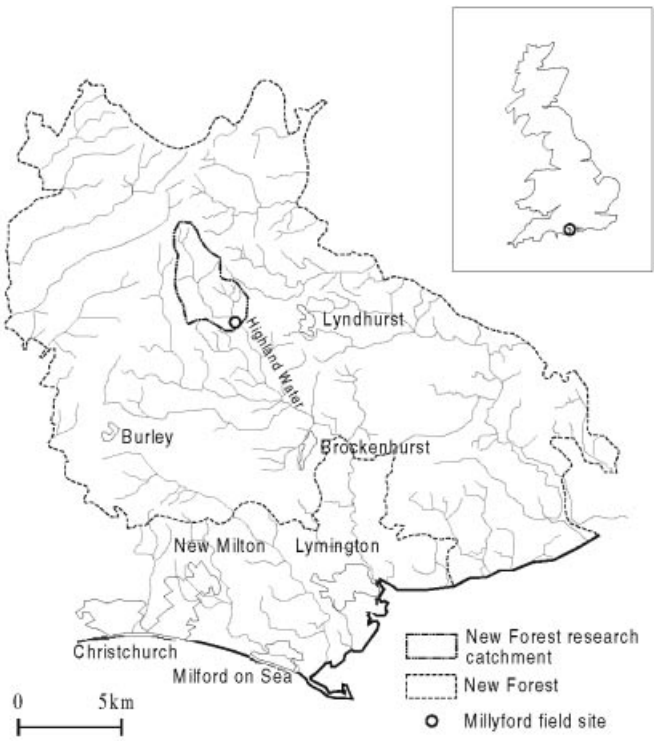

Figure 1. Map showing the location of the Highland Water

formulated that seek to explain pool–riffle maintenance. Of these theories a reversal in hydraulic conditions between pools and riffles arising from increasing discharge is most common. Various forms of hydraulic reversal have been suggested, including water surface slope (Keller, 1971), mean velocity (Lane and Borland, 1954; Keller and Florsheim, 1993), near-bed velocity (Keller, 1969, 1971; Carling, 1991; Carling and Wood, 1994) and shear stress (Lisle, 1979). Thompson *et al.*, (1996), referring to a specific pool morphology, revised the traditional velocity-reversal model to include the effects of recirculating eddies caused by a channel constriction at the pool head. These flow structures potentially explain why higher velocities are experienced in a pool in comparison to the adjacent riffles, despite their cross-sectional area being similar. The velocity-reversal with recirculating eddies model follows the inclusion of secondary flow cells to explain geomorphological behaviour (Bathurst, 1979). In this respect the theory links the concept of velocity-reversal with those which propose convergent and divergent flow patterns to explain pool–riffle development and maintenance such as Keller (1971). Keller (1972) suggested that the regular pattern of scour and deposition required for the formation of pools and riffles may be provided by an alternation of convergent and divergent flow patterns along the channel. Such conditions may be induced, even in straight channels, by curvature of streamlines along a meandering thalweg. This theory was further developed by Thompson (1986) to link secondary flow structures in pool–riffle sequences with meander development.

A review of the published data for sediment transport in pool–riffle sequences suggests that a velocity or bed shear stress reversal was not present at high flows for all cases and was therefore not the mechanism driving pool–riffle maintenance (Sear, 1996). In particular, there is little evidence for a reversal in the pool-tail, where sediment must be transported out of the pool, up a negative bed slope and onto the downstream riffle. The spatial and temporal resolution of the field evidence used to test reversal theories has, to date, been limited. Even the most detailed data set (Clifford and Richards, 1992) consists only of velocity measurements

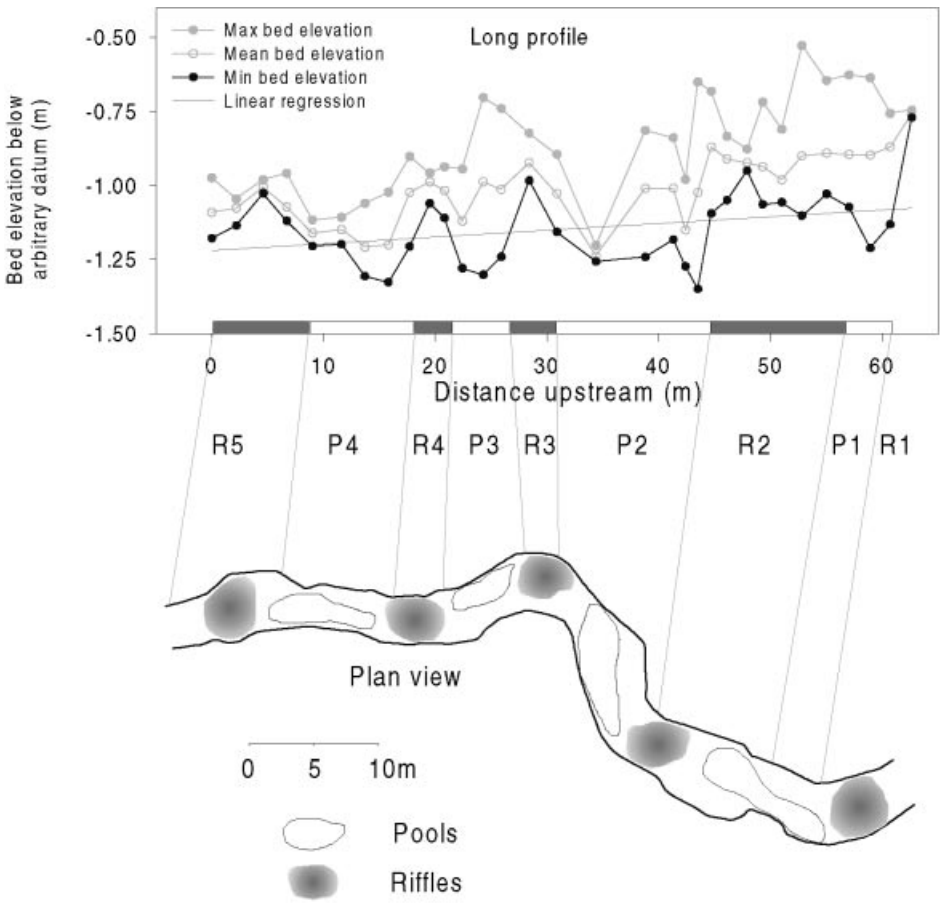

Figure 2. Pools and riffles at the Highland Water site within a bed profile, and the translocation of bedforms onto the channel planform

across two cross-sections in a pool and a further two on the adjacent riffle. The data were obtained for seven different, yet discrete discharges.

There is therefore a need for more detailed spatially distributed hydraulic data to enhance understanding of what is generally accepted to be a spatially distributed and stage-dependent system. However, field data acquisition at higher spatial and temporal resolutions is difficult. There are a number of high temporal and spatial resolution devices that can be used to collect hydraulic information. For example, acoustic Doppler current profilers (ADCPs); (e.g. Richardson *et al.*, 1996) or electromagnetic current meters (ECMs e.g. De Serres *et al.*, 1999). However, hydraulic measurements can only be taken in one place at a time. This is a major limitation when attempting to investigate spatially distributed phenomena and is especially true where flow is unsteady due to a changing hydrograph. In this case, attaining the required level of spatially distributed information within a short time period becomes a major constraint.

FIELD SITE AND MEASUREMENTS

The field site for this investigation is a 70 m reach of the Highland Water in the New Forest, Hampshire, UK. Figure 1 illustrates the location. Figure 2 shows a comparison of the position of pools and riffles based on the zero crossing method described by Milne (1982) using the channel long profile and observation in the field

Table I. Summary of site characteristics

Catchment area	12·7 km^2
Drainage density	2·18
Channel width	2·8 m
Bankfull depth	0·94 m
Bed slope	0·0085
$Q_{bankfull}$	2·2 $m^3 s^{-1}$
Maximum mean boundary shear stress (DuBoys method)	29·1 $N m^{-2}$
Maximum stream power	24·2 $W m^{-2}$
D_{16}	8·5 mm
D_{50}	18·6 mm
D_{84}	36·9 mm
Corey shape factor	0·52

based on sedimentological and low flow conditions. Table I gives a summary of the channel characteristics. The channel meanders with predominant geomorphological features including pools, riffles and point-bars. Clay geology at the site results in near-vertical bank profiles. The site has no bed vegetation although short grass and tree roots are present on the riverbanks. Typical net sediment transport at the site can be estimated from bedload trap contents which indicate that flow events are capable of transporting in excess of 50 kg of material through a cross-section (Sear *et al.*, 2000). CFD simulations were part of an integrated study of sediment transport processes at the site that included pebble tracing, repeated surveying of topography and bedload traps measurement. Pebble tracers were seeded across Riffle 2 at the site on 9 January 1999 and subsequently relocated. The tracers, manufactured to be of identical size, weight, shape and angularity, were designed to replicate the D_{16}, D_{50} and D_{84} of surface sediments at the site as shown in Table I. Results from bedload traps at the site showed that D_{16} size of tracer represents approximately the D_{65} of bedload transport at the site (Sear *et al.*, 2000).

Flow events at the site are of short duration; often peak discharge is maintained for less than 45 min. Hydraulic information for a near-bankfull, high flow event at the site was collected on 20 April 1999. One-dimensional measurements of streamwise velocity were carried out at 0·1 m intervals in the vertical for four velocity profiles across a pool and a riffle cross-section using a Braystoke current meter with a 0·06 m diameter impeller. Potentially hazardous wading was avoided by using a 6 m length of staging as a temporary bridge at both locations. Water surface elevations were also surveyed using an electronic distance measurer (EDM) (to an accuracy of $\pm$0·005 m). Measurements were taken at the peak of the hydrograph. Variation in stage during the time of all monitoring was less than 0·03 m. The peak discharge was calculated to be 1·88 $m^3 s^{-1}$.

An intermediate flow (0·91 $m^3 s^{-1}$) was monitored on 23 April 1999. On this occasion a Valeport Model 801 electromagnetic current meter was used allowing measurement of two-dimensional velocity vectors in the horizontal plane. Wading in the channel allowed measurement of velocity at an arbitrary height set to be 0·5 of the depth for locations distributed throughout the reach. Water surface elevation was measured at each of these locations. Velocity profiles were also collected at the centre of a pool and a riffle at measurement intervals of 0·05 m in the vertical. In addition four velocity profiles were measured for a pool-head cross-section located on a bend with a steep streamwise vertical gradient. A comparison of field observations and model calculations across this cross-section provides a stringent test of calculated hydraulics. The direction of velocity components was parallel and perpendicular to fixed cross-sections orientated at right angles to the banks (to an estimated accuracy of $\pm$5 °). These cross-sections were spaced at 1 to 2 m intervals throughout the reach. The measurements were recorded on the falling limb of the hydrograph. During the measurement period stage fell by a total of 0·03 m. On both days the location of all velocity measurements was recorded by attaching an EDM target reflector to the top of the flow meter wading rod. All velocity measurements were recorded over a 30 s time period.

Table II. Notation for SSIIM numerical symbols

C_μ $C_{\varepsilon 1}$ $C_{\varepsilon 2}$ = constants in k–ε model	u = fluctuating velocity
g = gravitational acceleration	u_* = shear velocity
Δh_{ij} = vertical movement for water surface calculation	v_T = turbulent eddy viscosity
K = constant in wall function	x = 3-d co-ordinate
k = turbulent kinetic energy (per unit mass)	z = co-ordinate in vertical direction
k_s = roughness height	ε = dissipation rate for k
l = difference in height of water surface at P_{ij}, and P_{ref}	∇ = gradient operator ($\delta/\delta x$, $\delta/\delta y$)
P = pressure (P_{ij} is extrapolated pressure at each cell, P_{ref} is the reference pressure)	δ_{ij} = Kronecker delta
	ρ = density
P_k = term for production of turbulence	σ_k, σ_ε = constant in the k–ε turbulence model
t = time	τ = boundary shear stress
U = average velocity	

MODEL DESCRIPTION

The CFD code used for this investigation was SSIIM (Olsen, 1996). The model has been applied to a number of engineering situations including flow modelling for estimation of spillway capacity (Olsen and Kjellesvig, 1998a), simulation of water and sedimentation in a sand trap (Olsen and Skoglund, 1994), simulation of scour around a cylinder (Olsen and Kjellesvig, 1998b) and simulation of flow dynamics in a river with large roughness elements (Olsen and Stokseth, 1995). The program solves the Navier–Stokes equations with a k–ε turbulence closure model on a three-dimensional non-orthogonal grid. SSIIM employs the Navier–Stokes equations for turbulent flow in a general three-dimensional geometry:

$$\frac{\partial U_i}{\partial t} + U_j \frac{\partial U_i}{\partial x_j} = -\frac{1}{\rho}\frac{\partial}{\partial x_j}(P\delta_{ij} + \rho\overline{u_i u_j}) \tag{1}$$

to obtain the water velocity. Non-compressible, constant-density flow is assumed. Symbol notation is given in Table II.

A control-volume approach is used for discretization of the equations. The default mechanism for pressure correction is the SIMPLE method (Patankar, 1980). This is used for coupling of all cells except those closest to the surface and allows calculation of a free water surface. The water surface is fixed at the downstream boundary where the pressure, P_{ref}, is taken as a reference pressure. A pressure deficit at each cell is then calculated by subtracting this reference pressure from the extrapolated pressure for each cell and used to move the water surface (Olsen and Kjellesvig, 1998b):

$$\Delta h_{ij} = \frac{l}{\rho g}(P_{ij} - P_{ref}) \tag{2}$$

The power law is used in the discretization of the convective terms. Further explanation of these numerical methods is given in Patankar (1980), Melaaen (1992) and Olsen (1991).

The k–ε model is used to calculate turbulent shear stress for three-dimensional simulations within SSIIM. The eddy–viscosity concept with the k–ε model is used to model the Reynolds stress term as illustrated in Equation 3 (where the first term on the right-hand side of the equation forms the diffusive term in the Navier–Stokes equation):

$$-\overline{u_i u_j} = v_T\left(\frac{\partial U_i}{\partial x_j} + \frac{\partial U_j}{\partial x_i}\right) - \frac{2}{3}k\delta_{ij} \tag{3}$$

The k–ε model simulates the eddy–viscosity as:

$$v_T = \mathrm{C}_\mu \frac{k^2}{\varepsilon} \tag{4}$$

where k is kinetic energy as defined by:

$$k \equiv \frac{1}{2}\overline{u_i u_j} \tag{5}$$

k is modelled as:

$$\frac{\delta k}{\delta t} + U_j\left(\frac{\delta k}{\delta x_j}\right) = \frac{\delta}{\delta x_j}\left(\frac{v_T}{\sigma_k}\frac{\delta k}{\delta x_j}\right) + \mathrm{P_k} - \varepsilon \tag{6}$$

where P_k is given by:

$$P_\mathrm{k} = v_\mathrm{T}\frac{\partial U_i}{\partial x_j}\left(\frac{\partial U_j}{\partial x_i} + \frac{\partial U_i}{\partial x_j}\right) \tag{7}$$

and ε is modelled as:

$$\frac{\partial \varepsilon}{\partial t} + U_j\frac{\partial \varepsilon}{\partial x_j} = \frac{\partial}{\partial x_j}\left(\frac{v_\mathrm{T}}{\sigma_\varepsilon}\frac{\partial \varepsilon}{\partial x_j}\right) + \mathrm{C}_{\varepsilon 1}\frac{\varepsilon}{k}\mathrm{P_k} - \mathrm{C}_{\varepsilon 2}\frac{\varepsilon^2}{k} \tag{8}$$

The influence of rough boundaries on fluid dynamics is modelled through the inclusion of the wall law:

$$\frac{U}{u_*} = \frac{1}{\mathrm{K}}\ln\left[\frac{30z}{k_s}\right] \tag{9}$$

as given by Schlicting (1979). The variable k_s equates to the roughness height. Boundary shear stress is calculated as:

$$\tau = 0 \cdot 3\rho k \tag{10}$$

(Olsen, personal communication, 1999). This approach is the one used by Olsen and Skoglund (1994) and Olsen and Kjellesvig (1998b) and assumes that turbulent kinetic energy is the driver for boundary shear stress. In open cells, turbulent kinetic energy can be advected with the flow and dissipated to adjacent cells. However, energy can not pass through bed cells and is assumed to be transferred from kinetic energy to a force in the form of boundary shear stress. Using this approach boundary shear stress is principally determined by shear near the bed through Equations 6 and 7.

SIMULATION OF HYDRAULICS IN A NATURAL POOL–RIFFLE SEQUENCE

Field data describing channel topography at the site were collected on 27 April 1999 using an EDM. This information was used to create the inputs required to run the model for the two monitored discharges. The bank outline was used to define the model's planform limit. Bed topography was measured at 292 positions on the bed chosen to describe changes in topographic gradient (point density of $0{\cdot}7\ \mathrm{m}^{-2}$). Topography was also measured for banks with sloping rather than vertical profiles. The channel topography for all grid points

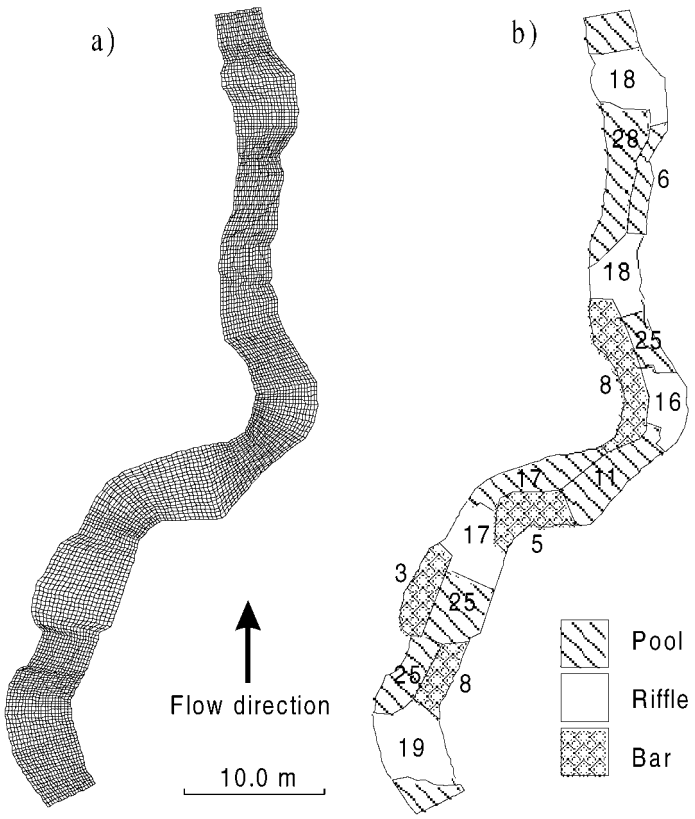

Figure 3. (a) Computational grid. (b) Delimitation of geomorphological units; numbers indicate D_{84} for samples of 100 particles (in mm)

was then obtained using a linear interpolation scheme. Figure 11a illustrates this bed topography. Measurements of 65 bank profiles at the site were used to incorporate complex bank topography into the model. Overhanging and irregular bank profiles were simulated by 'outblocking' areas of the numerical grid. The majority of banks were found to be near-vertical when measured and were therefore represented using vertical walls in the model. Figure 3a illustrates the computational grid used to simulate high flow at the site. This grid comprised 48 800 cells, 244 in the stream-wise, 20 in the cross-stream and 10 equally spaced in the vertical dimension. Each individual cell therefore represents a volume with approximate dimensions of 0·25 by 0·25 by 0·07 m (grid cell density 4 m^{-2}). Issues relating to grid quality are discussed by Lane and Richards (1998). The two numerical grids employed in this study were constructed following the guidelines provided by Bernard (1992) and employed by Lane and Richards (1998). Bernard (1992) recommended that the aspect ratio for two-dimensional models should not be more than 10 in areas where high gradients may occur. The greatest cell aspect ratios within the grid are the width/depth ratio of cells in the shallowest part of the model domain. The highest of these has a value of approximately 20. However, only 1·5 per cent of the model domain is above the recommended value of 10. Experiments showed that variation in near-bed cell size did not have significant effects on the near-bed hydraulic output, e.g. bed shear stress (Booker, 2000). For simulation of the intermediate flow a grid with a similar planform was used. This grid had nine cells in the vertical dimension. The near-bed cell in this simulation was set to be at 20 per cent of the flow depth, rather than 10 per cent for the high discharge, to maintain similar near-bed cell heights between the two model runs.

Resistance to flow in the form of boundary roughness is a boundary condition in the model. Bed roughness

Table III. Comparisons of measured and modelled water surface elevations for bank calibration (discharge is 1·88 $m^3 s^{-1}$). The Cal columns refer to calculated water surface elevations; Diff columns refer to measured elevations subtracted from modelled elevations; 25, 50 100 and 150 refer to the ks values used for bank roughness. All values are in metres. Locations of measurements are shown in Figure 4

Position	Cal 25	Diff 25	Cal 50	Diff 50	Cal 100	Diff 100	Cal 150	Diff 150
A	−0·279	−0·079	−0·274	−0·074	−0·248	−0·048	−0·208	−0·008
B	−0·3	−0·065	−0·295	−0·06	−0·272	−0·037	−0·236	−0·001
C	−0·3	−0·05	−0·295	−0·045	−0·273	−0·023	−0·239	0·011
D	−0·305	−0·079	−0·302	−0·076	−0·281	−0·055	−0·247	−0·021
E	−0·331	−0·044	−0·327	−0·04	−0·311	−0·024	−0·284	0·003
F	−0·33	−0·044	−0·326	−0·04	−0·31	−0·024	−0·284	0·002
G	−0·361	−0·057	−0·358	−0·054	−0·348	−0·044	−0·334	−0·03
H	−0·331	−0·043	−0·329	−0·041	−0·314	−0·026	−0·291	−0·003
I	−0·356	−0·054	−0·354	−0·052	−0·346	−0·044	−0·331	−0·029
J	−0·36	−0·051	−0·358	−0·049	−0·351	−0·041	−0·338	−0·028
K	−0·37	−0·017	−0·369	−0·016	−0·363	−0·01	−0·354	−0·001
L	−0·366	−0·027	−0·366	−0·027	−0·361	−0·022	−0·352	−0·013
M	−0·373	0·001	−0·372	0·002	−0·368	0·006	−0·363	0·011
N	−0·374	−0·034	−0·374	−0·034	−0·372	−0·032	−0·367	−0·027
O	−0·392	0·021	−0·392	0·021	−0·393	0·02	−0·394	0·019
Average		−0·041		−0·039		−0·027		−0·008

for this investigation was assumed to be constant within each pool, riffle or bar. Samples comprising 100 surface particles taken from the centres of each pool, riffle and bar were collected. Roughness height parameters were input to the model based on $3{\cdot}5D_{84}$, as suggested by Hey (1986) and supported by Clifford *et al.* (1992). Figure 3b illustrates the spatial distribution throughout the model domain. The delimitation of these units was done in the field based on bed topography and sedimentology. The precise definition used was that given by Raven *et al.* (1998): 'A riffle is a shallow, fast flowing water unit with a distinctive disturbed surface, forming upstream-facing unbroken standing waves, usually over gravel substrate. A pool is a distinctive feature of deeper water. Back currents are usually present. In dry weather conditions there is no perceptible flow.'

A comparison of pool–riffle delimitation using this definition with the more objective zero crossing method described by Milne (1982) and Carling and Orr (2000) showed no significant difference in the delimitation of pools and riffles at the site produced as shown in Figure 2.

Quantification of bank roughness is made difficult due to the presence of vegetation (Fischer-Antze *et al.*, in press) and variation in bank topography. A global value for bank roughness height was attained through a calibration process using comparisons of calculated and observed water surface elevations for the higher discharge (1·88 $m^3 s^{-1}$) event. This calibration procedure assumes that topography and discharge model boundary conditions that were measured in the field are correct. Table III illustrates the results of this calibration process. The calibration method assumes that the $3{\cdot}5D_{84}$ multiplier for bed roughness is correct and that discharge and channel topography are correctly represented in the model. The downstream model boundary corresponds to a rectangular concrete section in the field. This allowed water surface elevation at the downstream model boundary to be given a fixed value, measured by a pressure transducer (to an accuracy of 0·001 m), corresponding to the discharge and gained from measurement in the field.

Table III shows the rise in water surface elevations that result from an increase in bank roughness. Locations of water surface elevation measurements are shown in Figure 4. Using a value of 1·5 m for bank roughness, the model underpredicts measured water surface elevation by an average of 0·008 m. This discrepancy equates to less than 1 per cent of the total water depth. The difference between calculated and observed is arguably within the accuracy of the measurement if it is assumed that there is a possible ±0·005 m

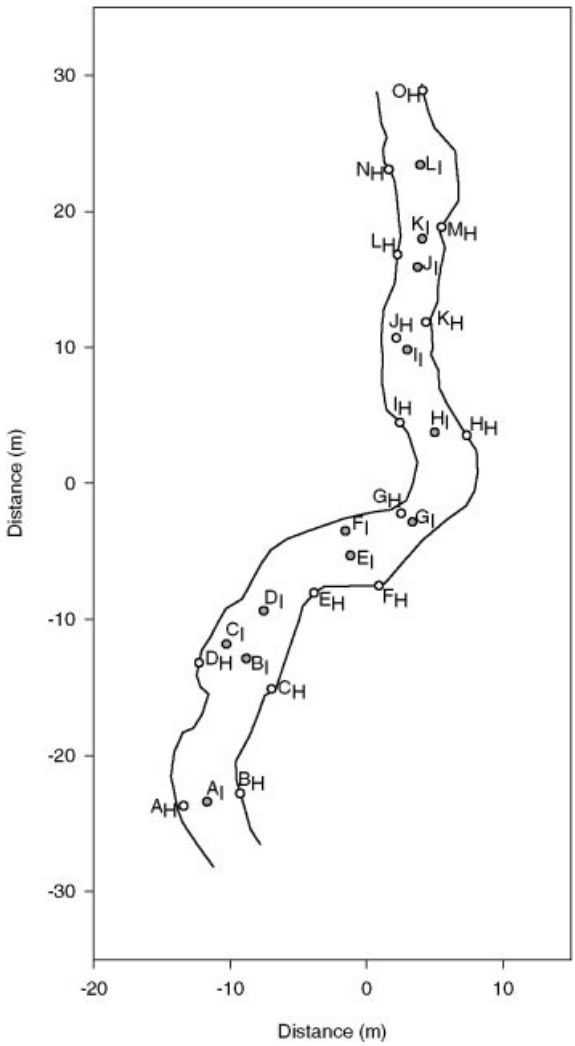

Figure 4. The locations of water surface elevation measurements. Subscripts indicate intermediate flow (0·91 $m^3 s^{-1}$) and high flow (1·88 $m^3 s^{-1}$) events. Flow direction is from bottom to top

precision error and a ±0·005 m systematic bias error for measurement of water surface elevation (Webster and Oliver, 1990).

Although the average difference between observed and calculated water surface elevation is small, there is spatial variation in the discrepancies between measured and calculated. Unsteady flow, spatially distributed bank roughness, the influence of woody debris in the channel, complex bank topography, and insufficient spatial resolution of bed topography are all possible explanations for these variations. For example, the apparent underprediction of water surface elevation along the left bank may be the result of a drop in flow occurring during the time it took to cross the river. Alternatively, a higher bank roughness along this bank could also be an explanation for the higher observed water surface. The same roughness was therefore used to simulate the intermediate flow that was monitored on 23 April 1999 to provide an independent assessment of the calibration process. The results are given in Table IV.

The discrepancy between calculated and observed water surface elevations at the upstream boundary of the

Table IV. Comparisons of measured and modelled water surface elevations for an intermediate flow (0·91 $m^3 s^{-1}$) using a bank roughness of 1·50 m. All values are in metres

Position	Measured	Modelled	Difference
A	−0·486	−0·53	−0·044
B	−0·541	−0·534	0·007
C	−0·527	−0·538	−0·011
D	−0·567	−0·551	0·016
E	−0·630	−0·601	0·029
F	−0·603	−0·604	−0·001
G	−0·621	−0·602	0·019
H	−0·644	−0·647	−0·003
I	−0·670	−0·666	0·004
J	−0·679	−0·667	0·012
K	−0·669	−0·67	−0·001
L	−0·696	−0·694	0·002
Average			0·002

intermediate flow simulation is an example of a model boundary effect. In reality there is a riffle upstream of the input boundary that increases the water surface elevation in the downstream adjacent pool. The effects of this riffle on the water surface elevation are not included in the model. Given this physical explanation, the discrepancy can be seen as a limitation of the modelling procedure rather than a consequence of any deficiency in the model program such as errors in model assumptions. At higher flow the effects of the upstream riffle are drowned out. Discarding the furthest upstream point gives an average model accuracy of 0·008 m for the water surface elevations for intermediate flow simulation.

Given the complexity of the channel topography, possible measurement error and the unsteady flow conditions, the level of correspondence for simulated water surface elevations was deemed to provide a simulation that was capable of representing the hydraulics in the river. A bank roughness of 1·50 m was therefore used. The apparently high value of bank roughness fulfils the function of retarding flow to a high degree in the cells nearest the banks such as might be expected in channels with rigid root structures in the banks, and as indicated by field measurements of near-bank velocities. Clearly, the specification of bank roughness within narrow channels with complex roughness elements generates problems for CFD boundary specification. In this case the right results may have been produced for the wrong reason. For example, the high roughness value may be compensating for an underestimation of channel width. In this case the bank roughness can be seen as functioning to narrow the channel. Whilst water surface elevation is sensitive to the value of bank roughness (and was therefore varied to calibrate the model) the paper focuses on the distribution of velocity, and in particular near-bed velocity, which was found to be insensitive to the chosen bank roughness value.

The patterns of velocity entering the model will affect results toward the upstream boundary of the model. As a result, measured velocity distributions for the input cross-sections (or inlet) are preferable for CFD simulations (Nicholas and Sambrook-Smith, 1999; Lane *et al.*, 1999). However, measurement of flow velocity for model verification was given priority over measurement of the upstream boundary condition during field measurement. The velocity distribution at the upstream boundary was measured for a discharge of 1·90 $m^3 s^{-1}$ on 24 October 1998. On this occasion a relatively uniform pattern of flow was evident across the cross-section. All simulations were therefore run using a uniform velocity pattern across the upstream boundary with a log profile in the vertical rather than a distribution of measured velocities. Experiments assessing the effect of the velocity distribution at the inlet showed that calculated velocity vectors in all three dimensions converged to within 0·01 m s^{-1} within 18 m of the

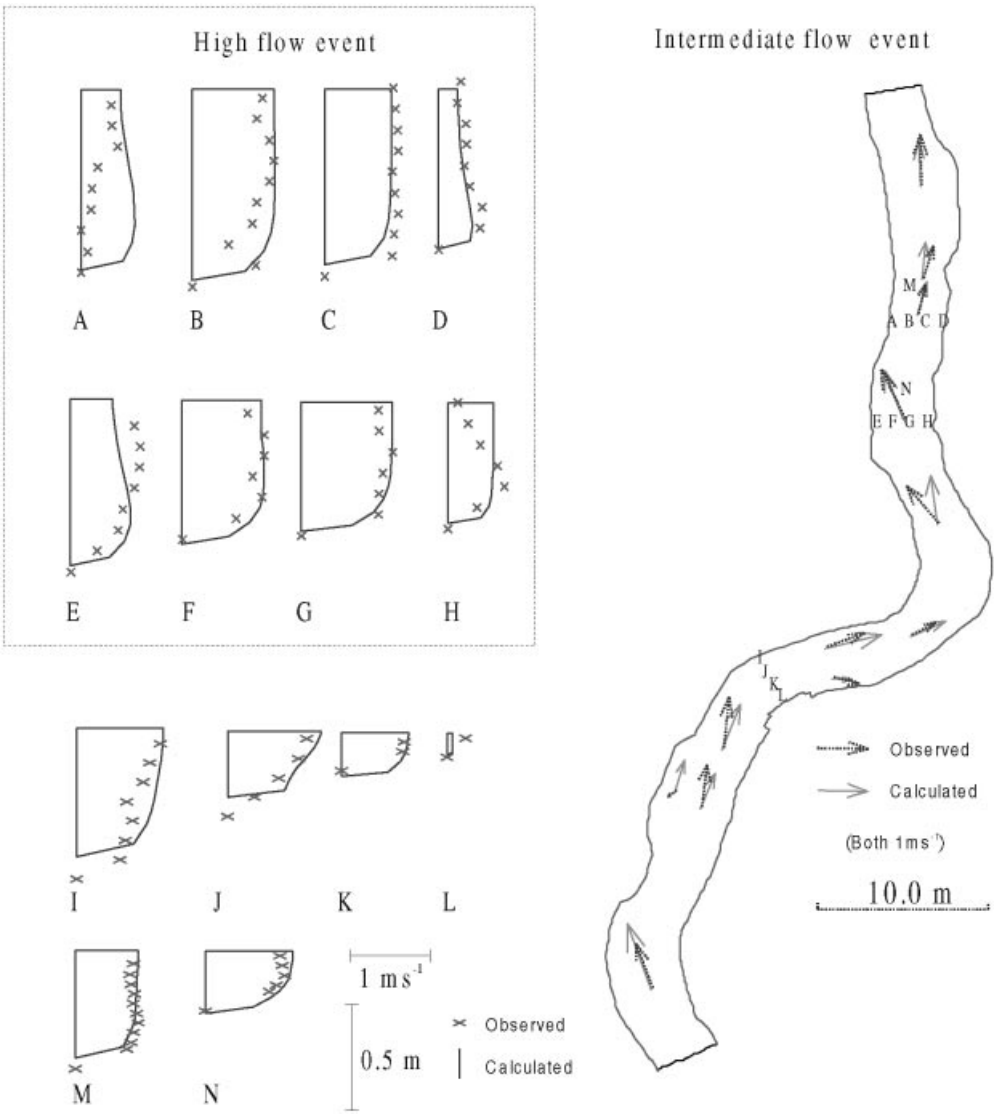

Figure 5. Comparison of calculated and observed velocity vectors. A–D and E–H illustrate velocity profiles in a pool and riffle cross-section respectively for the high flow event. M and N illustrate a detailed velocity profiles in a pool and riffle respectively for the intermediate flow event. I–L illustrate velocity profiles across a bend cross-section at intermediate flow. All locations are marked on the plan map

inlet even when the fastest velocity was skewed toward either bank and set to be 50 per cent of those at the opposite bank.

MODEL ASSESSMENT

Figure 5 illustrates comparisons of calculated and observed velocity profiles for both events. This figure also shows the position of each velocity measurement used to assess model calculations. Figure 6 shows a comparison of downstream velocity components measured for the near-bankfull flow with model

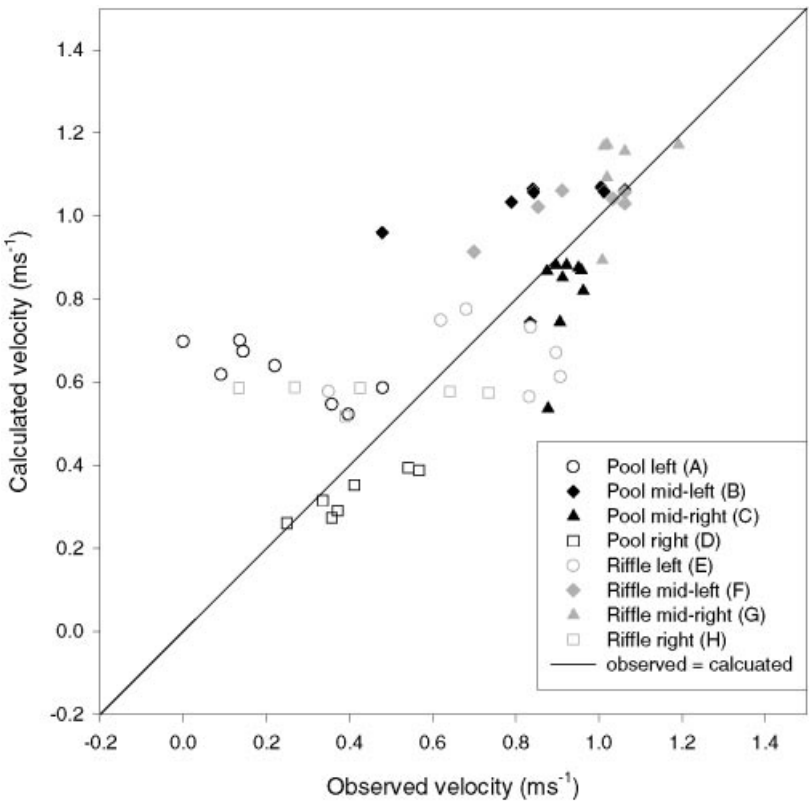

Figure 6. Comparisons of observed and calculated downstream velocity at high flow (1·88 $m^3 s^{-1}$). Letters refer to positions shown in Figure 5

calculations. The level of agreement for patterns of velocity through the pool and riffle cross-sections at high flow, in addition to the correspondence in water surface elevations, implies that some aspects of the spatial hydraulic patterns observed in the field are well represented in the model simulations. Cross-sectional comparisons of velocity suggest that the accuracy of model calculations becomes more reliable with distance from the bank. The discrepancies may be the result of fine spatial resolution variations in bank topography that are not included in the model. For example, a slight overhanging bank profile would cause the flow pattern observed at H. Least squares linear regression on all points in Figure 6 produces a line of best fit described by:

$$v_{cal} = 0{\cdot}583 v_{obs} + 0{\cdot}360 \tag{11}$$

with an r^2 value of 0·51 (sample size 59), where v_{cal} and v_{obs} are calculated and observed horizontal velocities respectively. However, when points in profiles measured at locations near the banks (A and H) are discarded from the analysis the line of best fit is:

$$v_{cal} = 0{\cdot}927 v_{obs} + 0{\cdot}061 \tag{12}$$

with an r^2 value of 0·65 (sample size 45). The relationship described by Equation 12 shows a good correspondence between observed and calculated downstream velocity. The difference in the level of correspondence between Equations 11 and 12 suggests that the model simulation produced a good representation of reality for six of the eight velocity profiles. However, profiles measured at A and H were not

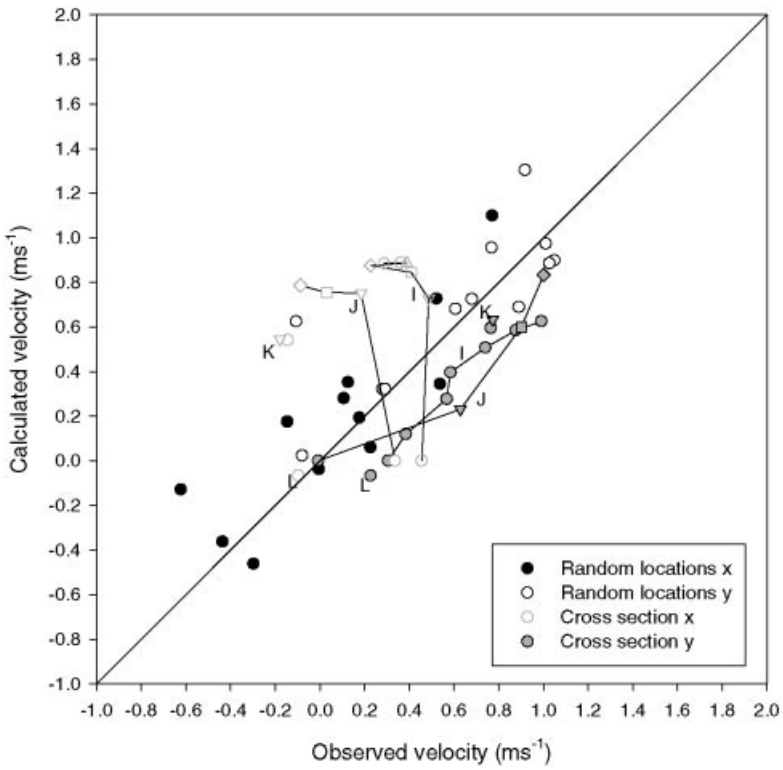

Figure 7. Comparison of observed and calculated results for all two-dimensional velocity measurements (discharge is 0·91 m s^{-1}). Grey points indicate velocity measurements constituting velocity profiles. The line joining these points indicates their order in the velocity profile with the circle representing the near-bed measurement. Locations (to which I–L refer) are marked on Figure 5

well replicated. The proximity of these profiles to the banks (less than 0·35 m) suggests that the differences between observations and calculations were caused by poorly constrained bank topography representation in the model. It should be stressed that differences between observations and calculations were present in the minority of the comparisons, and were limited to points near the banks. The consequences of possible deficiencies in bank topography specification are decreased near the bed where flow calculation is determined by both the bed and bank boundary conditions.

The velocity profile observations at a pool and a riffle, shown in Figure 5, for the intermediate flow, at M and N respectively, are particularly well replicated. The magnitude of velocity across the 'bend' cross-section is also well replicated by model calculations. There is also a high level of correspondence between observed and calculated flow direction. This is reflected in Figure 7, which illustrates correspondence for all two-dimensional velocity measurements. For this figure the velocity components were divided into x and y directions. These directions correspond to the arbitrary co-ordinate system illustrated in Figure 4 rather than stream-wise and cross-stream components. This method of comparison avoids determination of streamwise and cross-stream components. The figure shows that, for the velocity vectors that were recorded at half the depth and located throughout the model domain, there is a good correspondence between observations and calculations. The best fit line for these points is:

$$v_{cal} = 0{\cdot}838 v_{obs} + 0{\cdot}0154 \tag{13}$$

and has an r^2 value of 0·77 (sample size 24). This level of agreement corresponds well with published comparisons between CFD calculations and observed velocity. For example, Nicholas and Sambrook-Smith

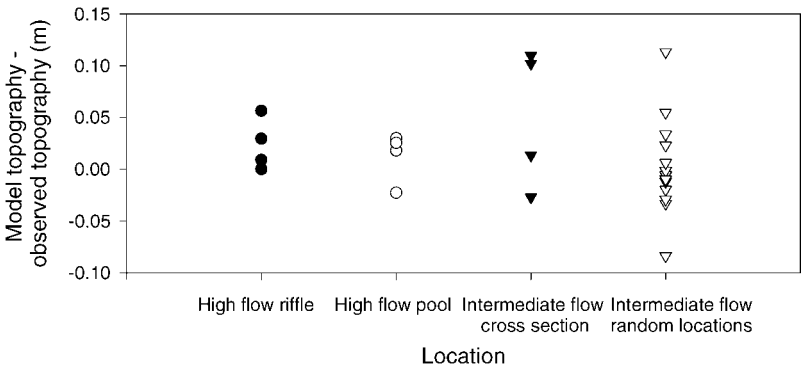

Figure 8. Comparison of topography included in the model and that observed at the time of velocity measurement at the high ($1{\cdot}88\ m^3\ s^{-1}$) and intermediate ($0{\cdot}91\ m^3\ s^{-1}$) flow

(1999) reported:

$$M = 0{\cdot}734P + 0{\cdot}104 \tag{14}$$

and

$$M = 0{\cdot}8P + 3{\cdot}62 \tag{15}$$

with r^2 values of 0·78 and 0·67 for P (calculated) and M (observed) speed and direction respectively. Hodskinson and Ferguson (1998) reported a relationship:

$$U_{cal} = 0{\cdot}89U_{obs} - 0{\cdot}0533 \tag{16}$$

where u_{cal} (downstream velocity component) had an r^2 value of 0·89 when correlated with field measurements. Similarly, Lane *et al.* (1999) quoted regression slopes (through the origin) of 0·86 and 0·66 with r^2 values of 0·71 and 0·77 for downstream and cross-stream velocities respectively.

The measurements that were located along the cross-section labelled I–J are spread further away from the line $y = x$. For these profiles velocity in the y-direction is calculated to within $0{\cdot}4\ m\ s^{-1}$ of the observed values. The x-velocity components in the deepest part of the channel display the largest discrepancies between observed and calculated, the maximum of which is approximately $0{\cdot}7\ m\ s^{-1}$. The source of the discrepancies could be attributed to a combination of CFD modelling phenomena that fall into two categories. The first source of possible error in model calculations is a deficiency in model assumptions such as the use of the two-equation k–ε model rather then a full Reynolds stress method for turbulence closure, or numerical errors, such as false diffusion (Olsen and Kjellesvig, 1998b). The second is model boundary conditions. These include errors in topography data collection and interpolation, insufficient representation of bank topography, the global bank roughness assumption, fixed bed roughness within each pool, riffle and bar. Given that field observations are well replicated in all locations other than those marked I and J in Figure 5 it seems likely that there is a localized factor that is causing the discrepancy rather than a flaw in the fundamental model assumptions. Field observations indicated that this location had the steepest stream-wise bed slope in the reach.

Figure 8 illustrates the discrepancies between bed topography measured at the time of hydraulic data collection and the topography that was set as a boundary condition in the model. The majority of points are represented in the model with an accuracy of $\pm 0{\cdot}025$ m and all but five are within $\pm 0{\cdot}05$ m. Depth at locations I and J is 0·11 and 0·10 m higher in the model than was measured in the field. This is further

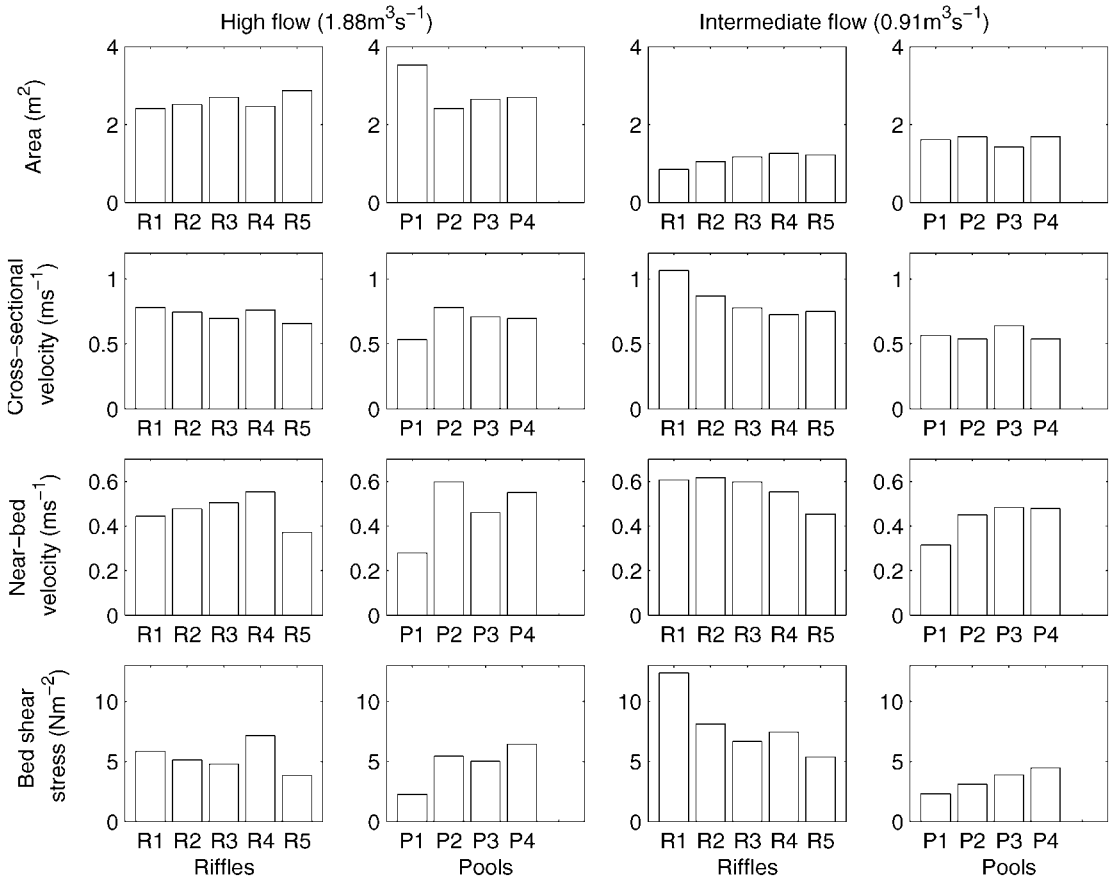

Figure 9. Cross-sectional area, velocity, average near-bed velocity and bed shear stress at mid-riffle and mid-pool cross-sections

evidence in support of the hypothesis that it is the model bed topography that is producing discrepancies between observed and calculated flow directions at locations I and J. It may be the case that secondary circulation being simulated in this pool has a realistic form but that the discrepancies between topography caused it to be slightly lagged in space. Inspection of the model output showed that the strength of the secondary circulation increases just downstream of I and J. Overall, the three-dimensional model simulations replicate the observed hydraulics although with local discrepancies.

RESULTS

Evidence for cross-sectional reversals in hydraulic parameters

The spatial limitations of field investigation have meant that to date theories such as velocity reversal have only been tested through comparison of hydraulic measurement along a cross-section. Model results can be analysed using the same method. Figure 9 illustrates a summary of the simulated hydraulics for mid-pool and mid-riffle cross-sections. The position of these cross-sections is illustrated in Figure 11a. Out of a total combination of eight pool–riffle couplets (e.g. Riffle 1 (R1) and Pool 1 (P1), Pool 1 (P1) and Riffle 2 (R2) etc.) from which evidence for a reversal in cross-sectional velocity might be obtained, three show reversals ($R2 < P2$ (5%), $P2 > R3$ (11%) and $R3 > P3$ (2%)). The percentage given after each couplet indicates the

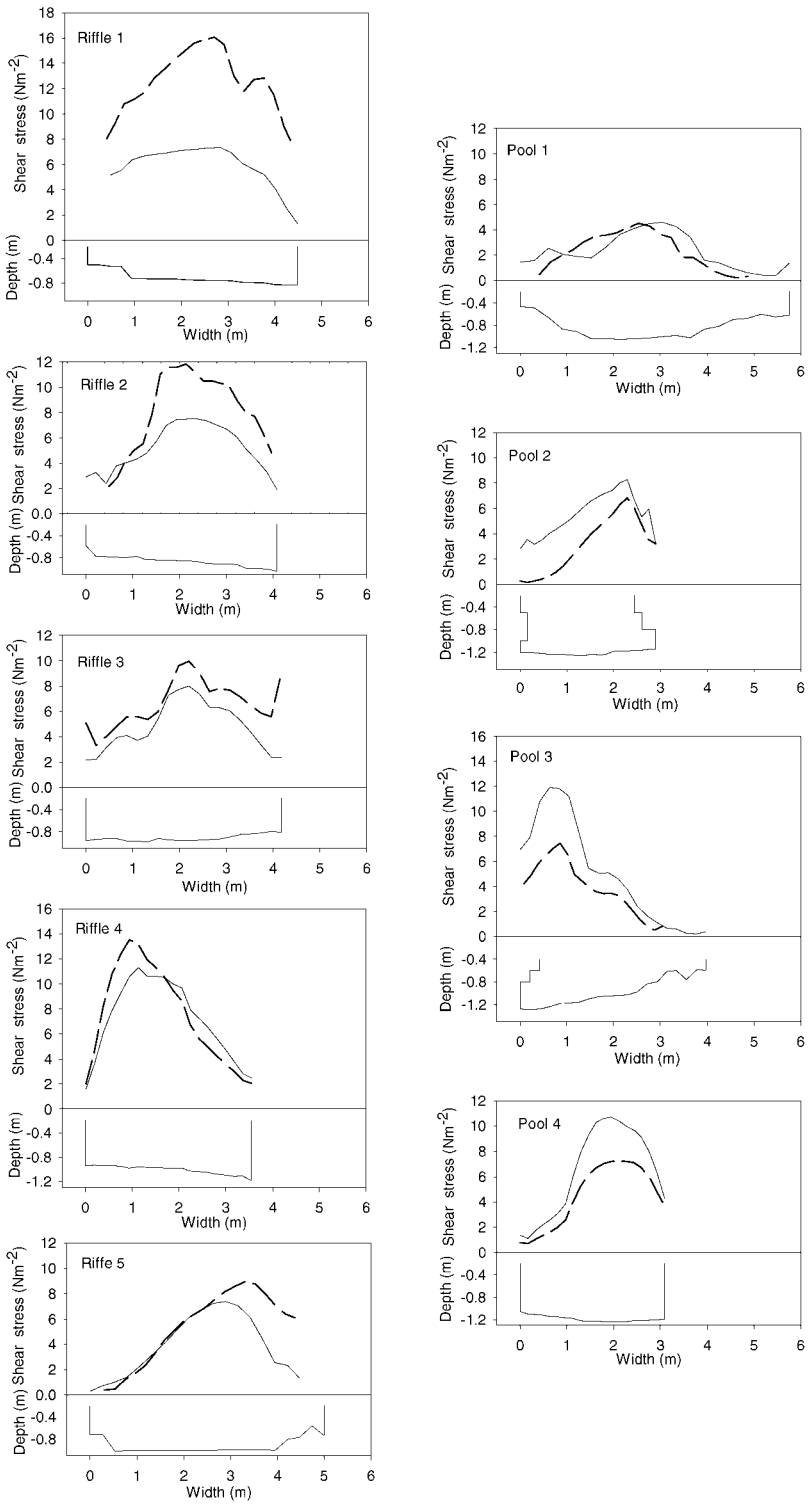

Figure 10. Cross-sectional variations in bed shear stress at the centre of pools and riffles. Solid lines indicate high flow ($1{\cdot}88\ m^3\ s^{-1}$), dashed lines indicate intermediate flow ($0{\cdot}91\ m^3\ s^{-1}$). Bed topography is shown below each bed shear stress plot. Cross-section locations are illustrated in Figure 11a. View is looking upstream

magnitude of reversal. Figure 9 shows that these three couplets are those which have pools with smaller cross-sectional areas than their respective adjacent riffles. The mechanism by which the reversals occurred is, however, different from the general velocity reversal theory where velocity in pools rises at a faster rate than at riffles (Clifford and Richards, 1992). Four of the five riffles experience a decrease in cross-sectional velocity at near-bankfull discharge in comparison to intermediate discharge. Cross-sectional velocity in Pool 1 (which has a relatively shallow, wide shape) is 6 per cent less at the near-bankfull discharge in comparison to the intermediate discharge, whilst Pools 2, 3 and 4 experience increases of 31, 10 and 23 per cent respectively.

Keller (1971) specifically utilized near-bed velocity as a surrogate for sediment transport competence and capacity to explain tracer pebble and grain size differences between pools and riffles. Figure 9 illustrates the same tendencies for near-bed velocity as cross-sectional velocity. Near-bed velocity at all riffles is greater for the lower discharge except for Riffle 4, where it remains constant. Pools exhibit more diverse behaviour. Pools 2 and 4 experience increased cross-sectional near-bed velocity whereas Pools 1 and 3 experience slight decreases at the higher discharge. With the exception of Pool 1, the magnitude of the decrease in riffle and increase in pool cross-sectional near-bed velocity is sufficiently large to produce comparable values in pools and riffles. Out of the eight pool–riffle couplet combinations, only three show reversals in cross-sectional mean near-bed velocity ($R2 < P2$ (25%), $P2 > R3$ (16%), $P4 > R5$ (33%)). Riffle 4 has a cross-sectional mean near-bed velocity that is only 0·5 per cent greater than Pool 4 indicating equalization of cross-sectional mean near-bed velocity for this couplet. The mechanism for these reversals is principally the result of a decrease in near-bed velocity at each riffle as discharge rises to near-bankfull. Analysis of the maximum near-bed velocities for the mid-pool and mid-riffle cross-sections showed further evidence for a reversal in near-bed velocity. With the exception of Pool 1 all mid-pool cross-sections exhibited a maximum near-bed velocity that was greater than or equal to those in both adjacent riffles.

Lisle (1979) and Carling (1991) recognized that a link exists between spatial patterns of bed shear stress and the transfer of sediment. Correspondingly a bed shear stress reversal or equalization theory was invoked to explain the maintenance of pool–riffle sequences. Figure 9 illustrates the average cross-sectional bed shear stress for the mid-pool and mid-riffle cross-sections. Bed shear stress is seen to decrease at riffles as discharge approaches bankfull. In contrast Pools 2–4 experience an increase in bed shear stress with increase in discharge. Pool 1 is again an exception as bed shear stress is similar at both discharges. Out of the eight pool–riffle couplets, four show reversals in cross-sectional mean bed shear stress ($R2 < P2$ (6%), $P2 > R3$ (12%), $R3 < P3$ (5%) and $P4 > R5$ (40%)).

Cross-sectional hydraulic variation was also present in the model output. Figure 10 illustrates the simulated bed shear stresses for the mid-pool and riffle-crest cross-sections for the high and intermediate flows. At the higher discharge riffles experience a uniformly distributed decrease in shear stress producing the same cross-sectional variation across the riffles for the two flows. This is in contrast with the higher discharge for pools where large increases are localized to the deepest parts of the pools rather than being uniformly distributed across the riverbed. Pools 2–4 have steep cross-stream gradients of bed shear stress and all the pools have zones of low bed shear stress. At pools 1 and 3 these lower zones correspond to the fine sediment bars whose locations are shown in Figure 3.

Spatial hydraulic patterns

Figure 11 illustrates simulated spatial patterns of near-bed hydraulics for the river at the two discharges. The figure shows that, in addition to the considerable cross-sectional hydraulic variation, as illustrated in Figure 10, there is also significant spatial variation in the downstream direction within each pool–riffle sequence. The scale at which the near-bed hydraulics vary highlights the spatial limitation of using at-a-point field hydraulic data for investigation of river channel hydraulics in pool–riffle sequences. Assuming that the model predictions are correct, cross-sectional variations can be missed from measurements at four points across a section. Given this degree of spatial variation in hydraulic patterns, and the limitations in the spatial distribution of information yielded from field investigation, it is perhaps understandable why there is a poorly

developed understanding of pool–riffle maintenance. The spatial variations illustrated in Figure 11 demonstrate the level of contingency that exists for hydraulic variations between pools and riffles in the river. For example, the area of higher near-bed horizontal velocity in Pool 2 appears to expand as flow increases whereas the opposite is true for Pool 3.

Analysis of Figure 11 illustrates some consistency in the changes in near-bed velocity that result from increased discharge with regard to pools and riffles. Overall, as discharge approaches bankfull, the width of the zone of higher near-bed velocity and bed shear stress increases at pool and riffles. This zone is clearly defined, but still occupies only 50 per cent of the flow width in places. This is opposite to the expected situation of broad zones of similar velocity across riffles and narrow concentrated zones of higher velocity in the deepest parts of pools. Planform controls on secondary flow clearly affect the migration of the zone of high bed shear stress through Riffle 3–4. As discharge rises, the inner bank zone of low bed shear stress extends upstream and widens downstream whilst it reduces at the outer bank as the high bed shear stress region migrates towards the right bank. It is interesting to note that the high near-bed velocity and bed shear stress zones all four pools and at Riffle 5 are confined by lower bed shear stress at the margin of the channel. In the pools these zones correlate with an increase in near-bed velocity and bed shear stress, whilst at Riffle 5, divergent flow over the riffle into a wider cross-section acts to reduce near-bed velocity and bed shear stress.

There is a downstream migration of the zones of faster near-bed velocity and bed shear stress in pools as the discharge increases. This migration is particularly evident in Pools 2, 3 and 4 where the region of higher near-bed velocity and bed shear stress extends downstream from the mid-pool into the pool-tail and connects onto the downstream riffle. At intermediate flows, the pool-head to mid-pool regions are generally associated with higher near-bed velocity and bed shear stress. Patterns of velocity at the pool-tail are of particular interest as a relatively high velocity is required here to explain pool maintenance. Specifically a high velocity is required to evacuate material out of the pool up a negative bed gradient to stop it from filling. Pools 3 and 4 both exhibit zones of high near-bed velocity at the pool exit. However, a zone of high pool-exit velocity is not so clearly present for Pools 1 or 2. This is consistent with field observations at the site that showed deposition of sediment in these two pools. It is possible that there is a threshold for the amount of deposition that can occur in pool tails above which velocity is increased and deposition can no longer occur. This theory is supported by the lack of significant topographic change in the position of pools and riffles over the two flood seasons prior to April 1999.

Overall the complexity of the spatial patterns in near-bed velocity and bed shear stress within the reach declines as discharge rises. Zones of higher bed shear stress extend and coalesce, whilst marginal recirculation zones and areas of relatively low bed shear stress generally reduce in area to form discrete locations for deposition. Decline in the near-bed velocity and bed shear stress on riffles reduces hydraulic differences between pools and riffles in the case of Riffle 2–Pool 2–Riffle 3, but reverses them in the case of Pool 4 and Riffle 5. Despite a high degree of convergence in mean flow parameters, as stage rises, considerable spatial variation still occurs at the reach scale.

Near-bed flow routing

Figure 12 illustrates patterns of near-bed flow direction for the two modelled flows. The velocity trajectories shown were calculated using a streamline function that interpolates near-bed flow direction from horizontal velocity vectors near the bed. The figure illustrates that near-bed velocity trajectories do not converge into pools as described by Keller (1971) although divergent flow over Riffle 5 is evident. Flow direction is skewed across the streambed away from the deepest part of pools as flow passes over the downstream slope of riffles and into pool-heads. The routing of flow away from the deepest parts of pools occurs in all four riffle–pool sequences in the model domain. This routing is more pronounced at the intermediate discharge in comparison to the higher flow due to stronger secondary circulation. However, even at the higher discharge routing is strongly represented. Trajectories that start at mid-riffle are routed away from the deepest part of pools to such an extent that for those starting on Riffles 1 and 2 no near-bed flow is routed directly into the downstream pool.

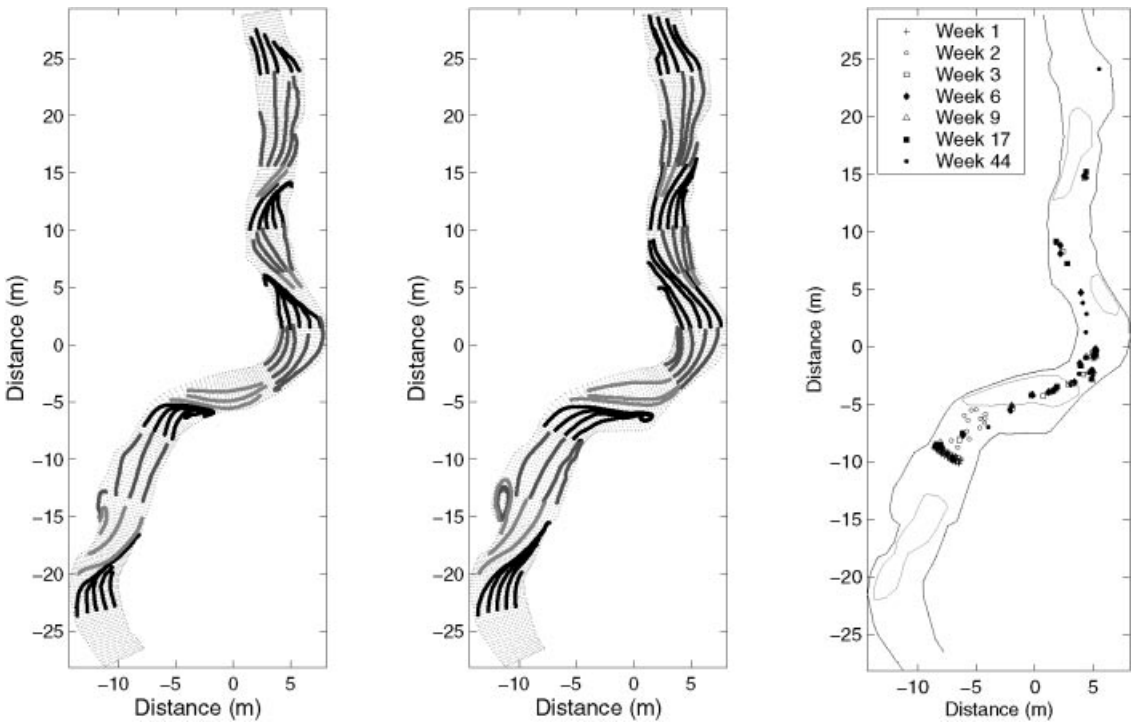

Figure 12. Horizontal flow trajectories near the bed. Intermediate (0·91 $m^3 s^{-1}$) and high (1·88 $m^3 s^{-1}$) flows are illustrated in the left-hand and middle diagrams, respectively. Trajectories starting in different locations are illustrated by different shades of grey: the darkest trajectories are those that start at mid-riffle, intermediate grey trajectories start at mid-pool and the lightest shade start at pool-head. The right-hand diagram shows the positions of tracers and pools at the site. Flow direction is from bottom to top

Figure 12 also shows the locations at which tracers, seeded Riffle 2, were found at the site. The figure shows that there was a distinct zone along which pebble tracers were deposited. The shape of this zone suggests that the tracers travelled along a particular route through the reach. There is a high level of correspondence between the pattern of modelled near-bed flow direction and the locations at which tracers were found. The path of the tracers shows that sediment in the reach was routed away from the head of Pool 2 and the deepest parts of Pools 3 and 4. The correspondence between the model near-bed flow direction and tracer positions can be seen as evidence that supports the assumption that sediment pathways correspond to near-bed velocity directions as well as an additional method of model verification.

CFD experiments of simple channel confluences by Bradbrook *et al.* (1998) demonstrate that a secondary circulation cell can be created where sufficient cross-stream momentum transfer results from channel asymmetry and the ratio of velocities between the two input channels. A similar explanation can be used to give a physical basis for the existence of secondary circulation in the relatively straight section of the Highland Water. Continuity of flow through a channel with alternating symmetrical riffles and asymmetrical pools causes differential pressure gradient along each pool-head cross-section and a singular secondary circulation cell that dictates the near-bed flow patterns illustrated in Figure 12. Low-amplitude meanders present in the modelled reach also contribute to the strength of the secondary circulation. The form of the three-dimensional flow patterns modelled for the Riffle 2 to Riffle 3 section of the river are illustrated in Figure 13. Figure 13 shows that secondary flow patterns are particularly strong in this section of the river at the head of Pool 2 (Figure 13b and c).

Figure 12 also illustrates the presence of a recirculation zone at the head of Pool 1 as described by Thompson *et al.* (1996). This recirculation zone is present at both intermediate and high discharges. The

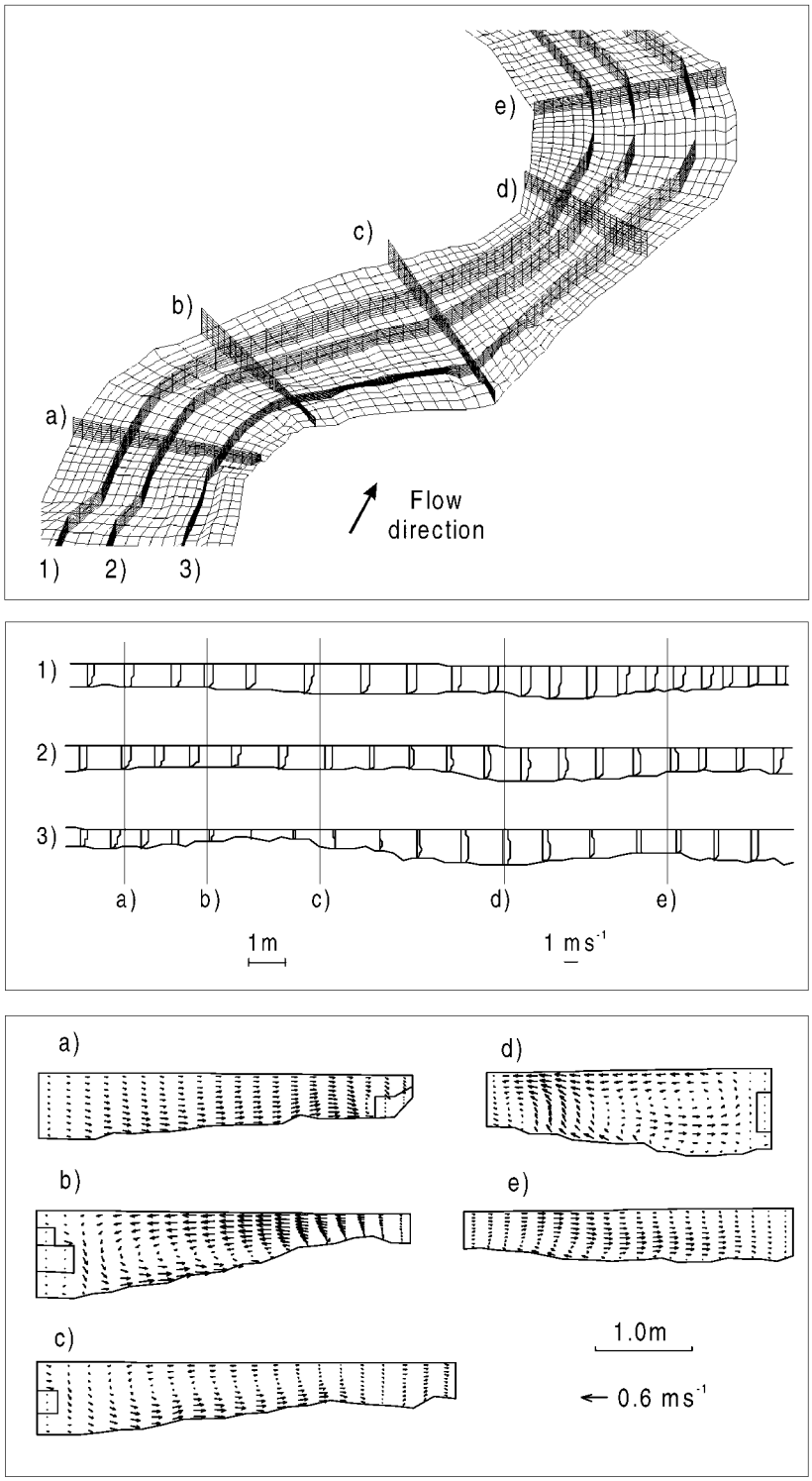

Figure 13. Visualization of three-dimensional flow through Riffle 2, Pool 2 and Riffle 3 (discharge 1·88 $m^3 s^{-1}$). Top: three-dimensional representation of the numerical grid. Middle: long profile with velocity vectors. Bottom: cross-sections with cross-sectional velocity vectors

strength and size of the zone increase as the discharge increases. The recirculation zone is the result of a constriction at the pool-head. The presence of the recirculation zone confirms that the Thompson *et al.* (1996) theory is a possible mechanism for the maintenance of Pool 1. The recirculation zone in Pool 1 has the effect of increasing velocity at the centre of that pool with a resulting increase in capacity to transport material out of the pool and maintain the morphology. There is the possibility that the recirculation zone at the head of Pool 1 may become stronger when the pool experiences deposition. As a result, velocity and bed shear stress would rise and enable maintenance of pool morphology. The other three pools in the simulation do not contain recirculation zones. This implies that the presence of recirculating zones at the pool-head is a phenomenon that may act to maintain pool morphology but is of secondary importance in comparison to sediment routing. In fact, in the case of Pool 1 the recirculation zone acts to increase the strength of flow routing away from the entrance of the pool and onto the adjacent bar.

DISCUSSION

The aim of this paper is to seek an explanation for the maintenance of a natural sequence of pools and riffles. Results show that there is evidence in support of hydraulic reversal theories. As discharge increases there is a decrease in cross-sectional velocity, near-bed velocity and bed shear stress on riffles. This supports the theory of bed shear stress reversal as a mechanism for pool maintenance (Lisle, 1979) and the deposition of coarser particles on riffles at high flows (Hirsch and Abrahams, 1981). However, the way in which the reversal occurs contradicts the theory outlined by Clifford and Richards (1992) who propose that reversal occurs because velocity, and therefore bed shear stress, rises at a slower rate at riffles than in pools. There is a physical explanation for the behaviour of bed shear stress predicted by the model. In the model, bed shear stress is a linear function of near-bed k (see Equation 10). Near-bed k is created principally by shear in the near-bed flow (see Equations 6 and 7). Changes in bed shear stress can therefore be interpreted as changes in near-bed flow: an increase in shearing at the bed will manifest itself as an increase in predicted bed shear stress. At a riffle, flow depth is increased by a factor of two between the two discharges. However, cross-sectional velocity falls slightly. There is therefore a reduction in shear as discharge increases so that predicted bed shear stress also falls. The cross-sectional velocity falls for higher flows because of increased bank roughness contribution. In pools the increase in flow depth is of the order of 30 per cent. Cross-sectional averaged velocity increases slightly. There is therefore an increase in shear as discharge increases and predicted bed shear stress consequently increases. In this case, the increase associated with deeper flow more than compensates the increased bank roughness contribution. Model experiments suggest that the phenomenon is not the result of model grid resolution as shear stress is not dependent on vertical grid resolution within the range of six to 12 cells equally spaced in the vertical dimension.

Reversals in cross-sectional velocity, near-bed velocity and bed shear stress were all evident in one or more, but not all, of the pools when compared to the adjacent upstream and downstream riffles. Analysis of model results therefore supports theories that suggest that an equalization or reversal between hydraulic characteristics was experienced in some but not all of the eight pool–riffle couplets. The results also indicate that high velocity at the pool-head can be caused by recirculating eddies.

Analysis of near-bed velocity patterns suggests that the direction of sediment routing is a strong influence on pool–riffle maintenance. Near-bed velocity patterns supported by results from tracing experiments suggest that near-bed flow direction can cause routing of sediment away from the deepest parts of pools. Patterns of near-bed velocity direction indicate flow routing away from the deepest part of pools as flows pass over the downstream slope of riffles and into pool-heads. Patterns of near-bed velocity direction therefore indicate maintenance of pool–riffle morphology by a lack of sediment being routed into pools rather than an increased ability to erode resulting from convergence of flow into the pool.

Pool maintenance as a result of sediment and near-bed flow routing that bypasses the deepest parts of pools negates the need for a hydraulic reversal mechanism which make comparisons between the magnitude of hydraulic variables at pool and riffle cross-sections. For example, the magnitude of section-averaged bed

shear stress in a pool at high flow compared to its adjacent riffles is not the primary mechanism for pool maintenance if sediment is being routed around the margin of that pool.

CONCLUSIONS

A CFD model is used to simulate the hydraulics of a mixed-sediment-size, natural pool–riffle sequence. Model inputs were gained from field measurements. The model calculations were tested against field observations and were found to produce discrepancies of similar magnitude to the measurement error for water surface elevations. The model also produced reasonable replication of measured velocity directions and magnitudes and in particular velocity profiles. The simulations suggest that as discharge increases, cross-sectional pool velocity increases and cross-sectional riffle velocity decreases. However, the magnitude of these changes is not sufficient to cause systematic velocity reversals in cross-sectional velocity. All mid-riffle cross-sections experienced a drop in bed shear stress with increasing discharge. These decreases were relatively uniformly distributed across the cross-sections. This is in contrast to the pools where bed shear stress increased as discharge increased. The largest increases were localized to the deepest parts of the pools. Further analysis revealed fine-resolution spatial variation of near-bed hydraulics.

The routing of near-bed velocity away from the deepest parts of pools was evident from analysis of near-bed velocity direction and has implications for sediment transport and the subsequent maintenance of pool–riffle morphology. Routing of sediment to bypass pools in combination with the lack of a systematic reversal in the magnitude of any of the hydraulic conditions (such as velocity and bed shear stress) suggest secondary circulation and near-bed flow direction are strong influences on pool–riffle maintenance in a relatively deep narrow channel. Further research is required to test the extent to which the generality of this routing hypothesis extends to rivers with higher width:depth ratios and sinuosities.

Analysis of the spatial hydraulic patterns demonstrated that generalized descriptions of pool–riffle hydraulics patterns, such as velocity reversal, are too simplistic to explain maintenance of all pool–riffle sequences. Complex patterns are particularly evident in pools where zones of high near-bed velocity were found to migrate downstream at greater discharge. Pool–riffle sequences are spatial phenomena and an understanding of the spatial as well as temporal variation in hydraulics is required to increase our understanding of their development and maintenance. As a result, future conceptual models which seek to explain pool–riffle maintenance must include analysis of changes in downstream spatial hydraulic patterns and, in particular, near-bed velocity direction with changes in discharge.

ACKNOWLEDGEMENTS

This paper benefited from constructive comments from Professor Stuart Lane and an anonymous referee. The research was conducted whilst D.J.B. was a postgraduate student at the Department of Geography, University of Southampton. Field assistance was provided by Matthew Cole, Richard Jeffries, Gary Llewellyn, Mark Skelton, Andy Tatem and Katherine Townsend. The CFD code employed in the study was made available by Nils Olsen.

REFERENCES

Bathurst JC. 1979. Distribution of boundary shear stress in rivers. In *Adjustments of the Fluvial System*, Rhodes DD, Williams GP (eds). Kendall-Hart: Dubuque, Iowa; 95–116.

Bernard RS. 1992. *STREMR: numerical model for depth-averaged incompressible flow*. Technical Report HY-105. US Army Corps Engineers: Waterways Experiment Reseach Station, Vicksburg, Mississippi.

Booker DJ. 2000. *Modelling and monitoring sediment transport processes in pool-riffle sequences*. PhD Thesis, Department of Geography, University of Southampton.

Bradbrook KF, Brion PM, Lane SN, Richards KS, Roy AG. 1998. Investigation of controls on secondary circulation in a simple confluence geometry using a three-dimensional numerical model. *Hydrological Processes* **12**: 1371–1396.

Brookes A. 1995. Challenges and objectives for Geomorphology in U.K. river management. *Earth Surface Processes and Landforms* **20**: 593–610.

Brookes A.: 1996. Floodplain restoration and rehabilitation. In *Floodplain Processes*, Anderson MG, Walling DE, Bates PD (eds). John Wiley & Sons: Chichester; 553–576.
Carling PA. 1991. An appraisal of the velocity reversal hypothesis for stable pool/riffle sequences in the River Severn, England. *Earth Surface Processes and Landforms* **16**: 19–31.
Carling PA, Orr HG. 2000. Morphology of riffle-pool sequences in the river Severn England. *Earth Surface Processes and Landforms* **24**: 369–384.
Carling PA, Wood N. 1994. Simulation of flow over pool-riffle topography: a consideration of the velocity reversal hypothesis. *Earth Surface Processes and Landforms* **19**: 319–332.
Clifford NJ. 1993. Differential bed sedimentology and the maintenance of riffle-pool sequences. *Catena* **20**: 447–468.
Clifford NJ, Richards KS.: 1992. The reversal hypothesis and the maintenance of pool-riffle sequences: a review and field appraisal. In *Lowland Floodplain Rivers: Geomorphological Perspectives*, Carling PA, Petts GE (eds). John Wiley & Sons: Chichester; 43–70.
Clifford NJ, Robert A, Richards KS. 1992. Estimation of flow resistance in gravel-bed rivers: a physical explanation of the multiplier of roughness length. *Earth Surface Processes and Landforms* **17**: 111–126.
De Serres B, Roy AG, Biron PM, Best JL. 1999. Three-dimensional structure of flow at a confluence of river channels with discordant beds. *Geomorphology* **26**: 313–335.
Fischer-Antze T, Stosser T, Bates P, Olsen NRB. (in press). 3D numerical modelling of open-channel flow with submerged vegetation. *Journal of Hydraulic Research*.
Hey RD. 1986. River mechanics. *Journal of the Institute of Water Engineers and Scientists* **40**: 139–158.
Hey RD. 1992. Environmentally sensitive river engineering. In *The Rivers Handbook: Hydrological and Ecological Principles*, Callow P, Petts GE (eds). Blackwell Scientific Publications: Oxford; 337–362.
Hirsch PJ, Abrahams AD. 1981. The properties of bed sediments in pools and riffles. *Journal of Sedimentary Petrology* **51**: 757–760.
Hodskinson A, Ferguson RI. 1998. Numerical modelling of separated flow in river bends: Model testing and experimental investigation of geometric controls on the extent of flow separation at the concave bank. *Hydrological Processes* **12**: 1323–1338.
Keller EA. 1969. *Form and Fluvial Processes of Dry Creek, near Winters, California*. MS Thesis, University of California, Davis.
Keller EA. 1971. Areal sorting of bed material: the hypothesis of velocity reversal. *Geological Society of America, Bulletin* **83**: 915–918.
Keller EA. 1972. Development of alluvial stream channels, a five stage model. *Geological Society of America Bulletin* **83**: 1531–1536.
Keller EA, Florsheim JL. 1993. Velocity reversal hypothesis: A model approach. *Earth Surface Processes and Landforms* **18**: 733–740.
Lane SN. 1998. Hydraulic modelling in geomorphology and hydrology: A review of high resolution approaches. *Hydrological Processes* **12**: 1131–1150.
Lane EW, Borland WM. 1954. River-bed scour during floods. *Transactions, American Society of Civil Engineers* **119**: 1069–1079.
Lane SN, Richards KS. 1998. High resolution, two-dimensional spatial modelling of flow processes in a multi-thread channel. *Hydrological Processes* **12**: 1279–1298.
Lane SN, Bradbrook KF, Richards KS, Brion PA, Roy AG. 1999. The application of computational fluid dynamics to natural river channels: three-dimensional versus two-dimensional approaches. *Geomorphology* **29**: 1–20.
Lisle TE. 1979. A sorting mechanism for a riffle-pool sequence. *Geological Society of America Bulletin* **90**: 1142–1157.
Melaaen MC. 1992. Calculation of fluid flows with staggered and nonstaggered curvilinear nonorthogonal grids-the theory. *Numerical Heat Transfer* Part B **21**: 1–19.
Milne JA. 1982. Bed material size and the pool-riffle sequence. *Sedimentology* **29**: 267–287.
Nicholas AP, Sambrook-Smith GH. 1999. Numerical simulation of three-dimensional flow hydraulics in a braided river. *Hydrological Processes* **13**: 913–929.
Olsen NRB. 1991. *A three dimensional numerical model for simulation of sediment movements in water intakes*. Dissertation for Dr. Ing. degree, The Norwegian Institute of Technology, Division of Hydraulic Engineering, University of Trondheim, Norway.
Olsen NRB. 1996. A three-dimensional numerical model for simulation of sediment movements in water intakes with multi-block option. *SSIIM Users Manual Version 1·4*.
Olsen NRB, Kjellesvig HM. 1998a. Three-dimensional numerical flow modelling for estimation of spillway capacity. *Journal of Hydraulic Research* **36**: 775–784.
Olsen NRB, Kjellesvig HM. 1998b. Three-dimensional numerical flow modelling for estimation of maximum local scour depth. *Journal of Hydraulic Research* **36**: 579–590.
Olsen NRB, Skoglund M. 1994. Three-dimensional numerical modelling of water and sediment flow in a sand trap. *Journal of Hydraulic Research* **32**: 833–844.
Olsen NRB, Stokseth S. 1995. Three-dimensional numerical modelling of water flow in a river with large bed roughness. *Journal of Hydraulic Research* **33**: 571–581.
Patankar SV. 1980. *Numerical Heat Transfer and Fluid Flow*. McGraw-Hill: New York.
Raven PJ, Holmes NTH, Dawson FH, Kox PJA, Everard M, Fozzard IR, Rouen KJ. 1998. *River Habitat Quality: the physical character of rivers and streams in the UK and Isle of Man*. Report No. 2 to the Environment Agency.
Richards KS. 1976. Channel width and the riffle-pool sequence. *Geological Society of American Bulletin* **87**: 883–890.
Richardson WR, Thorne CR, Mahood S. 1996. Secondary flow and channel changes around a bar in the Barmaputra river, Bangladesh. In *Coherent Flow Structures in Open Channels*, Ashworth PJ, Bennett SJ, Best JL, McLelland SJ (eds). Wiley & Sons; Chichester: 519–543.
Schlicting H. 1979. *Boundary-Layer Theory*. McGraw-Hill: New York.
Sear DA. 1996. Sediment transport processes in pool–riffle sequences. *Earth Surface Processes and Landforms* **21**: 241–262.
Sear DA, Newson MD, Brookes A. 1995. Sediment related river maintenance: the role of fluvial gemorphology. *Earth Surface Processes and Landforms* **20**: 629–647.
Sear DA, Damon W, Booker DJ, Anderson DG. 2000. A load cell based continuous recording bedload trap. *Earth Surface Processes and Landforms*.

Thompson AT. 1986. Secondary flows and the pool-riffle unit: a case study of the processes of meander development. *Earth Surface Processes and Landforms* **11**: 631–641.
Thompson DM, Wohl EE, Jarrett RD. 1996. A revised velocity-reversal and sediment-sorting model for a high-gradient, pool-riffle stream. *Physical Geography* **17**: 142–156.
Webster R, Oliver MA. 1990. *Statistical Methods in Soil and Land Survey*. Oxford University Press; New York.

